BR8818377

PUBLICAÇÕES

IFUSP/P-688

POTENTIAL "ANOMALIES" IN $^{14}N + ^{27}Al$, ^{28}Si AND ^{29}Si SYSTEMS

E. Crema; J.C. Acquadro; R. Liguori Neto;
N. Carlin Filho and M.M. Coimbra

Instituto de Física, Universidade de Sao Paulo

Janeiro/1988

POTENTIAL "ANOMALIES" IN ^{14}N + ^{27}Al, ^{28}Si AND ^{29}Si SYSTEMS

E. Crema; J.C. Acquadro; R. Liguori Neto;
N. Carlin Filho and M.M. Coimbra

Departamento de Fisica Nuclear
Instituto de Fisica, Universidade de São Paulo
C.P. 20516, São Paulo, Brasil

ABSTRACT - We measured seven elastic angular distributions and the fusion excitation functions for the $^{14}N + ^{27}Al$, $^{14}N + ^{28}Si$ and $^{14}N + ^{29}Si$ systems within the energy range $1.1<E_{CM}/V_B<2.5$. The experimental fusion cross sections were superestimated by the simple one-dimensional barrier penetration model, with a "frozen" nuclear proximity potential. Through an effective variation of barrier height, we calculated the energy dependent corrections necessary to fit the data. These corrections showed an "anomalous" behaviour in the above-barrier energy region. The corresponding imaginary potential parts were then constructed through the use of dispersion relation.

1. - Introduction.

In the last years, a great amount of fusion excitation functions for light and medium weight systems were measured[1], yielding a natural division into two energy regions in the popular $1/E_{CM}$ plot. One of them, so-called region I, extends from roughly 1.1 to 2.0 times the Coulomb barrier energy. In this region the fusion cross section accounts for most of the total reaction cross section. It has been considered that the fusion in this region is governed only by the properties of the interaction barrier of the entrance channel[2]. In the other region, extending up from t i s the Coulonb barrier (so-called region II) the data show that, light systems such as the ones presented here, the fusion cross ion decreases or remains roughly constant with increasing bombarding energy, while the total reaction cross section continues to rise. or heavier systems, the fusion cross section still increases, as ene increases, but much more slowly than the total reaction cross section.

Until now, the strong limitation in light nucleus fusion in region II had basically two kinds of tentative explanation: the entrance channel models and, alternatively, the compound nucleus models. In the former, the fusion cross section is explained in terms of the general characteristics of the interacting nuclei in the entrance channel. Through the explicit or implicit use of both conservative and dissipative forces these models account for most of the gross features of the fusion excitation function[1]. There is the critical distance model[3], the critical nuclear charge superposition model[4], the critical nuclear mass superposition model[5], the finit friction model[1], the extra-push model[6], and the dinucleus doorway model[7]. In the latter, the fusion cross sections are explained via two kinds of compound nucleus models: (1) the extreme yrast line model[8] and the statistical yrast line model[9] both of which assume that there is an angular momentum limitation imposed by the compound nucleus; and (2) the Vandenbosch model[10] which assumes a critical level density in the compound nucleus, for each angular momentum that contribute to the fusion, so that a superposition of levels is guaranteed.

Nevertheless, in spite of the large amount of fusion measurements in light systems, and the large amount of theoretical tentatives to explain the fusion cross section limitation in region II, this region is still not well understood. Since the deep inelastic collisions appear to be the dominant channels competing with fusion in region II[1,11], a large amount of direct process measurements will be necessary to understand the origin of the fusion limitation in this region.

Concurrently with the above, there has been much effort concentrated in the study of the fusion between two heavy ions at energies near the Coulomb barrier (region I and below). In this energy region, the fusion cross section of several systems are much larger than those predicted by a simple Barrier Penetration Model (BPM)[12],where the nuclear potential used in the calculation is determined by the experimental data above the barrier. This fusion enhancement has been successfully predicted by calculations that couple the fusion directly to the non-elastic channels[12-14], which, in spite of being energetically closed at these energies, can favour fusion through virtual excitations. The global effect of these couplings can be represented by a renormalization of the unidimensional, real barrier potential[15-16].

More recently, it has been shown[17] that a simple BPM is adequate to exhibit the fusion enhancement due to the channel coupling, if the threshold anomaly is considered. These studies take into account the overall effect on fusion due to the coupling with all possible direct non-elastic channels without extensive computational calculations.

On the other hand, V.L.M. Franzin and M.S. Hussein[18] proposed a slightly different v to treat the heavy ion fusion enhancement. The fusion cross section, σ_F, is given by the following partial wave sum representation

$$\sigma_F = (\pi/k_0^2) \sum_{\ell=0}^{\infty} (2\ell+1)\ T^F(V_B+\Delta V^F) \qquad (1)$$

where V_B is an appropriate static, energy independent barrier and the transmission coefficients are given by the Hill and Wheeler expression

$$T_\ell^F(V_B+\Delta V^F) = \left\{ 1 + \exp\left[\frac{2\pi}{\hbar\omega} (V_B+\Delta V^F(E) + \frac{\hbar^2(\ell+\frac{1}{2})^2}{2\mu\ R_B{}^2} - E) \right]\right\}^{-1} \qquad (2)$$

where R_B and $\hbar\omega$ are the position and curvature barrier, respectively, and they are taken to be energy and angular momentum independent for sake of simplicity. By extracting the energy-dependent correction to the "frozen" proximity potential used in a one-channel description of fusion, they constructed the corresponding imaginary component of the interaction potential, using an inverse dispersion relation:

$$\Delta W^F(E) = -\frac{P}{\pi} \int \frac{\Delta V^F(E')}{E' - E} \, dE' \qquad (3)$$

where P means the principal value of the integral.

We turn now to lighter systems. Can we apply that heavier system potential analyses for lighter systems? What we can learn about the light system potentials using the dispersion relation? To be more specific, we consider here the $^{14}N + ^{27}Al$, $^{14}N + ^{28}Si$ and $^{14}N + ^{29}Si$ systems which are presented in this work. For our measured systems, we observe that the experimental fusion cross sections are overestimated by the BPM, when a "frozen" nuclear proximity potential (determinated from above barrier data) is used. In other words, following the language presently used for heavy systems one can say that there is a fusion hindrance in these light systems at energies near and above the Coulomb barrier (where experimental data are available).

Our experimental data were analyzed with a refinement of the method proposed in ref.18, and our $\Delta V^F(E)$ and $\Delta W^F(E)$ values, obtained from the experimental data, also exhibit an "anomalous" behaviour at energies near the Coulomb Barrier. It was also possible to connect the theoretical fusion values $\Delta W^F(E)$ with $\Delta W^D(E)$ values related to non-elastic direct reactions.

This work is structured in the following way: in Sec.2 the experimental procedure is briefly described; Sec.3 is dedicated to the presentation of the measurements and the results obtained; in

Sec.4 we discuss the method used to extract the $\Delta V^{F}(E)$ values from our experimental data; in Sec.5 we present the determination of the imaginary potential variation through an inverted dispersion relation; Sec.6 is dedicated to discussion of our results; and, finally, Sec.7 is a summary.

2. - Experimental Procedure.

For these measurements we used a ^{14}N beam extracted from the Pelletron Accelerator of the Universidade de São Paulo[19]. The ^{27}Al, ^{28}Si and ^{29}Si targets (isotopically enriched to 99.99%) had nominal thicknesses of 70,30 and 30 $\mu g/cm^2$, respectively. The Si targets were supported on 20 $\mu g/cm^2$ ^{12}C foil, and every target had a 2 $\mu g/cm^2$ Au layer ^{12}C was the main target contaminant.

Reaction products were identified by a E - ΔE proportional telescope: the residual energy signals were produced by a surface barrier detector with 100μm of nominal thichnesse and the energy loss signals were produced by proportional counter with 10 Torr of P-10. In addition to beam integration, one solid state detector was fixed at 15^{o} to provide an alternative normalization with elastically scattered events.

3. - Measurements and Results.

A. Fusion Cross Section.

A typical two-dimensional E - ΔE spectrum for the system $^{14}N + ^{29}Si$ is shown in figure 1. In spite of large $Z < 13$ fusion residue production, due mainly to the ^{12}C backing, identification of residues $Z > 13$ is easy, except in a small lower E region of the spectra where Z identification is impossible with this kind of detector. In these cases, the contaminant counts of $^{14}N + ^{12}C$ fusion were measured separately for some energies and the Sc residues delimitation could be estimated in those regions. The contaminant free region of the spectra always accounted for more than 95% of the total fusion counts.

In the $^{14}N + ^{27}Al$ spectra, with self-supporting aluminum targets, the Z<13 residue counts are neglegible and the ^{41}Ca residues identification was made without difficulty.

According to statistical model calculation (code LILITA[20]) for ^{42}Sc evaporation, with the maximum excitation energy of our measurements, the probability for the $Z = 13$ residue production is smaller than 1%.

The uncertainties in the absolute values of the total fusion cross section are due to counting statistics (1% to 4%); to the contaminant superposition estimated in the $^{28,29}Si$ cases (<5%); to charge integration (<3%); to solid angle and target thicknesses (<5%); to the extrapolation of the angular distribution to unmeasured angles (<3%); and, in the monitor normalization cases, to the monitor counting statistics (<3%) and to the monitor solid angle and target thicknesses (<3%). The total uncertainties in the absolute fusion cross section were estimated between 4% and 9%.

Seven fusion angular distributions were measured in the angular range $2.5^{o} < \theta_{LAB} < 40^{o}$ in steps of 2.5^{o} and 5^{o}. The fusion excitation functions were completed at only one angle measurements ($\theta_{LAB} = 7.5^{o}$). The fusion excitation functions for the studies systems are shown in figure 2.

B. Elastic Scattering.

The angular distributions for the elastic scattering were measured simultaneously with the fusion measurements in the forward angles ($\theta_{LAB}<40^{o}$) and with silicon detectors at larger angles. The angular distributions are shown in figure 3 where the lines are fits with the optical model using the parameters of table I. At our bombarding energies, these parameters are energy-independent.

4. - Extraction Of $\Delta V^{F}(E)$ Correction From Experimental Data.

A. The Nuclear Potential Choice.

The expressions 1 and 2 were used to obtain the empirical value $\Delta V^{F}(E)$, where we considered the position and curvature barrier dependencies on the angular momentum, to be evaluated by calculating

$$\frac{d}{dr}\left[U_N(r) + U_C(r) + \frac{\hbar^2\ell(\ell+1)}{2\mu r^2}\right]_{r = R_{B,\ell}} = 0 \qquad (4)$$

and $$(\hbar\omega_\ell)^2 = \frac{h^2}{\mu}\left\{\frac{d^2}{dr^2}\left[U_N(r) + U_C(r) + \frac{\hbar^2\ell(\ell+1)}{2\mu r^2}\right]\right\}_{r = R_{B,\ell}} \qquad (5)$$

where $U_N(r)$ and $U_C(r)$ are the nuclear and Coulomb potentials, respectively, μ is the reduced mass and $R_{B,\ell}$ is the Coulomb barrier position corresponding to the ℓ partial wave.

In heavy systems, the nuclear potential determination in these analyses is easy: one particular type of nuclear potential is chosen and its geometry is determined through the fitting of the above-barrier experimental data (where virtual excitations of non-elastic channels leading to fusion are negligible). In light systems, that high-energy reference choice is a little more delicate. For example, a direct comparison of the three systems that we studied reveals that above $E_{CM} \approx 35$ MeV the $^{14}N + {}^{28}Si$ excitation function differs from the $^{14}N + {}^{27}Al$, ^{29}Si systems, and it leads to a maximum fusion cross section 150mb greater than the other two systems. Therefore, the geometry of the proximity potential that we used was fixed by fits of the experimental data at energies around twice the Coulomb barriers ($E_{CM} \approx 35$ MeV), where we expect that the principal non-elastic channels are already energetically open and the phenomena responsible for the fusion limitation (in the so-called region II of the excitation function) are still not very important. These fits were obtained with $\Delta R = 0$[21] for the three systems and the BPM results with these proximity potentials are given in figure 2 (solid lines). We can state that, contrary to the heavy system cases, these light systems exhibit a hindrance of fusion with respect to the BPM prediction at energies near and above the Coulomb barrier.

B. The Method Of $\Delta V^F(E)$ Extraction.

The Wong model[22], with the parameters of the table II, predicted the experimental results nicely, as seen in figure 2. In order to simplify, we used the Wong predictions with "data" (with a small extrapol… on in the lower energy region). Using expressions 1-5 we calculated the empirical values $\Delta V^F(E)$ that equalize the BPM result with the data for each energy. Obviously, the BPM predictions with the energy dependent barrier coincide with the Wong fits in figure 2, and the correction values $\Delta V^F(E)$ responsible for these fits are shown in fig 4.

Figure 4 demonstrates the presence of an "anomalous" behaviour in real potentials at energies above and near the Coulomb barrier (≈20 MeV), such as the anomaly observed in elastic scattering of several systems[23], in spite of the opposite sign. Besides, we can see in figure 4 that the $\Delta V^F(E)$ of the $^{14}N + {}^{28}Si$ system shows an energy variation sharper than that for $^{14}N + {}^{29}Si$, it is even sharper than the $\Delta V^F(E)$ energy variation for the $^{14}N + {}^{27}Al$ system. As we will see later, these differences could be associated with different target deformation parameters.

5. - Theoretical Values Of $\Delta W^F(E)$.

We used the inverted dispersion relation (eq. 3) proposed in ref.18 in order to calculate the variation of the imaginary potential part responsible for the flux absorption in the fusion channel. That integral was solved with the aid of $\Delta V^F(E)$ polynomial fits suggested by Mahaux et al[17]:

$$\Delta V^F(E) = \begin{cases} 0 & E<E_a \\ \sum_m b_m(E-E_a)^m & E_a \leq E \leq E_b \\ 0 & E>E_b \end{cases} \tag{6}$$

where b_m, E_a and E_b are constants easily determined through polynomial fitting of $\Delta V_F(E)$ values in figure 4. In this way, equation 3 becomes simpler[18]:

$$\Delta W^F(E) = -\frac{1}{\pi}\left\{ \sum_{m=1}^{3} b_m(E-E_a)^m \ln\left|\frac{\Delta - (E-E_a)}{E - E_a}\right| + \right.$$

$$\left. + \sum_{m=1}^{3} b_m \sum_{\ell=0}^{m-1} (E-E_a) \frac{\Delta^{m-\ell}}{m-\ell} \right\} \tag{7}$$

where $\Delta = E_b - E_a$ and a three degree polinomial was used.

The results of the formal expression for the studied systems are shown in figure 4, where we can also observe an "anomalous" behaviour, in spite of the inverted sign with respect to the threshold anomaly exhibited by elastic optical potential of the other systems[17,23].

Therefore, our light system experimental data indicate that, while the real nuclear potential becomes more attractive, the imaginary potential part (responsible for the absorption of the flux that penetrates the barrier) becomes less absorptive with the bombarding energies above the Coulomb barrier.To understand this decrease in the imaginary part at energies above the Coulomb barrier, it is necessary to analyze the structure of the entire imaginary potential that acts during the ion interaction.

6. - Discussion.

For a given optical potential[24] of the type $U_\alpha = V_\alpha + iW_\alpha$, the total reaction cross section is given by the expectation value of W_α

$$\sigma_R = -(2/hv) \langle \chi_\alpha^{(+)} | W_\alpha | \chi_\alpha^{(+)} \rangle \quad , \qquad (8)$$

that computes the total flux lost from the entrance channel α, where $\chi_\alpha^{(+)}$ is the relative-motion outgoing-wave solution for channel α (generated by U_α) and v is the relative velocity in the channel α.

Since $\sigma_R = \sigma_F + \sigma_D$, where σ_F is the total fusion cross section and σ_D is the total absorption cross section in non-elastic (direct) channels, one can postulate[24)]

$$W_\alpha = W_F + W_D \qquad (9)$$

where W_F is associated with the fusion process, and W_D with the non-elastic direct ones. Since the optical model analyses of the elastic scattering data give the whole value of the W_α (and V_α), only the elastic scattering data can not be enough to reveal the mechanism responsible for the elastic optical potential anomaly. This aim can be attained if the elastic data are analyzed in conjunction with fusion or non-elastic reaction data.

In our studied energy regions, in spite of the lack of elastic experimental data in backward angles (figure 3), the optical model analyses reveal that the W_α are energy independent for all three systems, if the potential geometries are kept constants. So, we can write that $\Delta W_\alpha/\Delta E = 0$. And, with the aid the equation 9, we can say that for our especific cases,

$$\Delta W_F = - \Delta W_D \; . \qquad (10)$$

In spite of the energy independence of W_α, the individual pieces W_F and W_D have an anomalous behaviour at energies above the Coulomb barrier that mask each other and can not be observed in W_α. Figure 5 shows the sums $W_\alpha + W_D$ (that would have the energy variation on the direct imaginary potential, W_D), which show the same anomaly displayed by the elastic imaginary optical potential of several systems[17,23)]. This behaviour is expected: with the energy increase above the barrier more and more direct channels have been opened and the W_D part must be more absorptive.

Following this point of view, the elastic optical potential for these light systems at energies near the Coulomb barrier could exhibit an "anomalous" behaviour if W_D is neglegible (all non-elastic direct channels closed). So, the W_a energy dependence could be used as an indirect indicator of the existence of open non-elastic channels at sub-barrier energies.

Finally, we can also see in figure 5 the different absorption increases among the systems as the energy increases. This behavior is consistent with the different target deformation parameters. The larger deformation parameter of the $^{14}N + ^{28}Si$ system (β_N=-0.42) could facilitate the direct rotational excitations, and this could explain the more rapid increase of the direct absorption in the $^{14}N + ^{28}Si$ system compared to the other systems. It would be interesting to measure the inelastic scattering in order to verify this theoretical result. It would also be necessary to obtain experimental data for the other non-elastic channel to confirm our theoretical results.

7. - **Summary**.

Using a ^{14}N beam extracted from the Pelletron Accelerator of Universidade de São Paulo, we measured fusion and elastic scattering in the $^{14}N + ^{27}Al$, $^{14}N + ^{28}Si$ and $^{14}N + ^{29}Si$ systems, within the energy range $1.1 < E_{CM}/V_B < 2.5$. With an appropriate definition of an energy reference, we fixed the "frozen" nuclear proximity potential to be employed in the one-dimensional barrier penetration calculations. We found that these systems showed a hindrance of experimental fusion cross sections with respect to the BPM results. In order to fit our data with the BPM, it was necessary to make energy dependent correction of real potential barrier heights. These empirical corrections showed an "anomalous" behaviour at above Coulomb barrier energy region, with the same characteristics of the anomalies observe. in heavier systems, despite the opposite signs. So, we used an inverted dispersion relation to calculate the variation on the ima -ary potential part related to fusion processes. Obviously, those rea. potential variations were related to this fusion imaginary part of the potentials by the dispersion relation. But, in our case, we could not observe these variations in optical potentials obtained from the elastic scattering analyses. It was suggested that this is due to complementary behaviour of two imaginary potential pieces, responsible for flux absorption in the fusion channel and in non-elastic direct channels. This complementary behaviour can be understood as a flux conservation impositior.

We were able to infer what could be the variations of direct imaginary potential parts, and we found that they present an "anomalous" behaviour similar to the threshold anomalies observed in the optical potential of several systems. Despite the differences among the deduced direct imaginary potential parts, they are, however, consistent with different target deformations.

ACKNOWLEDGMENTS

We are indebted to M.S. Hussein for suggestions and for helpful discussions. We are also grateful to C. Tenreiro for providing the program KATTI.

REFERENCES

1. J.R. Birkelund and J.R. Huizenga.
   Ann. Rev. Nucl. Part. Sci. 33(1983)265.

   P. Frobrich.
   Phys. Reports 116(1984)337.

   D.H.E. Gross and H. Kalinowski.
   Phys. Reports 45C(1978)175.

2. H.H. Gutbrod, M. Blann and W.G. Winn.
   Nucl. Phys. A213(1973)267.

3. D. Glas and U. Mosel.
   Nucl. Phys. A237(1975)429.

4. D. Horn and J.A. Ferguson.
   Phys. Rev. Lett. 41(1978)1529.

5. M. Lozano a[illegible] G. Madurga.
   Phys. Lett. [illegible]B(1980)50.

6. W.J. Swiat[illegible]
   Physica Scr[illegible] 24(1981)113.

   S. Bjornholm and W.J. Swiatecki.
   Nucl. Phys. A391(1982)471.

7. O. Civitarese, B.V. Carlson, M.S. Hussein and A. Szanto de Toledo.
   Phys. Lett. 125B(1983)22.

8. M. Conjeaud, S. Gary, S. Harar and J.P. Wieleczko
   Nucl. Phys. A309(1978)515.

9. S.M. Lee, S.T. Matsuse and A. Arima.
   Phys. Rev. Lett. 45(1980)165.

10. R. Vandenbosch.
Phys. Lett. 87B(1979)183.

R. Vandenbosch and A.J. Lazzarini.
Phys. Rev. 23C(1981)1074.

11. D.H.E. Gross and H. Kalinowski.
Phys. Lett. 48B(1974)302.

12. "Fusion Reactions Below the Coulomb Barrier"
Lecture Notes in Physics, V.219, Ed. by S.G. Steadman
(Springer-Verlag, Berlin, 1985).

13. R.A. Broglia, C.H. Dasso, S. Landowne and A. Winther.
Phys.Rev. C27(1983)2433;

C.H. Dasso, S. Landowne and A. Winther.
Nucl.Phys. A405(1983)381.

R. Lindsay and N. Rowley.
J.Phys. G: Nucl.Phys. 10 (1984)805.

14. M.J. Rhoades-Brown and P. Braun-Munzinger.
Phys.Lett. 136B(1984)19.

15. N. Takigawa and G.F. Bertsch.
Phys.Rev. C29(1984)2358.

16. C.H. Dasso and S. Landowne.
Phys.Lett. 183B(1987)141.

17. C. Mahaux, H. Ngô and G.R. Satchler.
Nucl.Phys. A449(1986)354.

G.R. Satchler, M.A. Nagarajan, J.S. Lilley and I.J. Thompson.
Ann.Phys. 178(1987).

18. V.L.M. Franzin and M.S. Hussein.
Preprint - IFUSP - 596(1986). To be published.

V.L.M. Franzin.
São Paulo Ph.D. Thesis 1987 , unpublished.

19. O. Sala and G. Spalek.
Nucl.Instr. & Meth., 122(1974)213.

20. J. Gomes Del Campo, R.G. Stokstad, J.A. Biggerstaff, R.A. Dayras, A.H. Snell and P.H. Stelson.
Phys.Rev. C19(1979)2170.

21. L.C. Vaz, J.M. Alexander and R.G. Satchler.
Phys.Rep. C69(1981)373.

22. C.Y. Wong.
Phys.Rev.Lett. 31(1973)766.

23. J.S.Lilley, B.R. Fulton, M.A. Nagarajan, I.J. Thompson and D.W. Banes.
Phys. Lett. 151B(1985)181.

B.R. Fulton, D.W. Banes, J.S. Lilley, M.A. Nagarajan and I.J. Thompson.
Phys. Lett. 162B(1985)51.

A. Baeza, B. Bilwes, R.Bilwes, J. Dias and J.L. Ferrero.
Nucl. Phys. A419(1984)412.

24. T. Udagawa, B.T. Kim and T. Tamura.
Phys.Rev. C32(1985)124.
M.S. Hussein.
Phys.Rev. C30(1984)1962.

FIGURE CAPTIONS

Figure 1. The E x ΔE spectrum for the $^{14}N + ^{29}Si$ system at $E_{LAB} = 56$ MeV and $\theta_{LAB} = 7.5^{o}$.

Figure 2. Experimental fusion cross sections. The solid lines are the barrier penetration model prediction using a proximity potential with $\Delta R = 0$. The dotted lines are the Wong fits with the parameters of table II, and they are coincident with the barrier penetration model with the energy dependent corrections on barriers.

Figure 3. Elastic scattering angular distributions measured for a) $^{14}N + ^{27}Al$; b) $^{14}N + ^{28}Si$; and c) $^{14}N + ^{29}Si$ systems. The solid curves are best fits obtained from optical model calculations using the energy independent potentials of table I.

Figure 4. The energy dependent correction to barrier heights necessary to fit the data with BPM; and the calculated energy variations of imaginary potential parts related to the fusion process.

Figure 5. The calculated ' aginary potential parts related to the direct reactions.

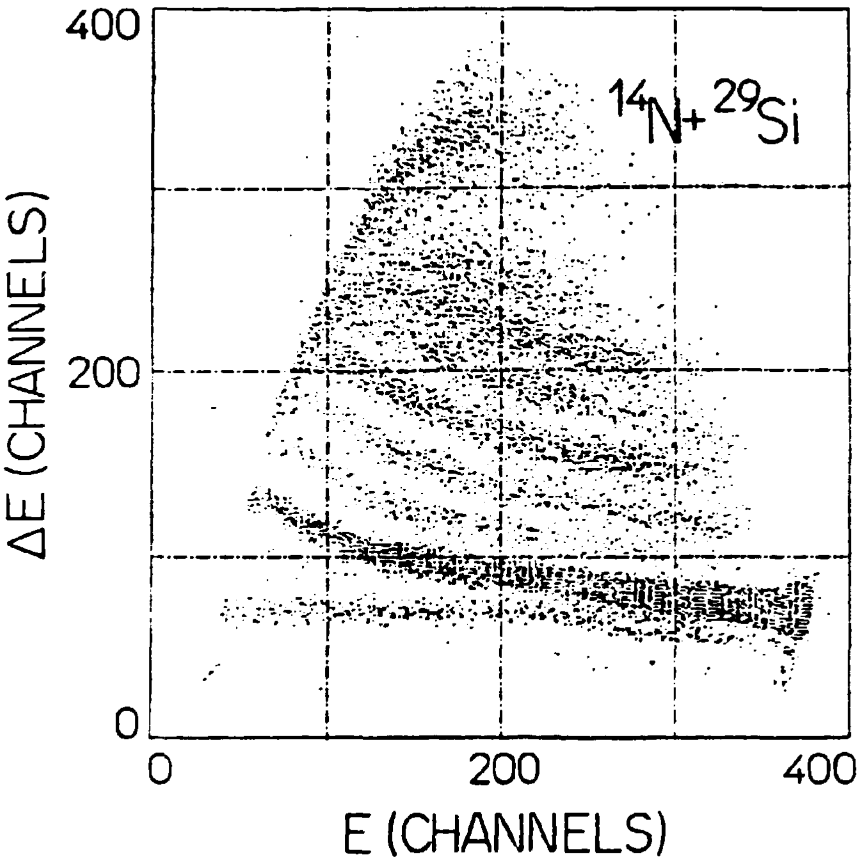

Figure 1.

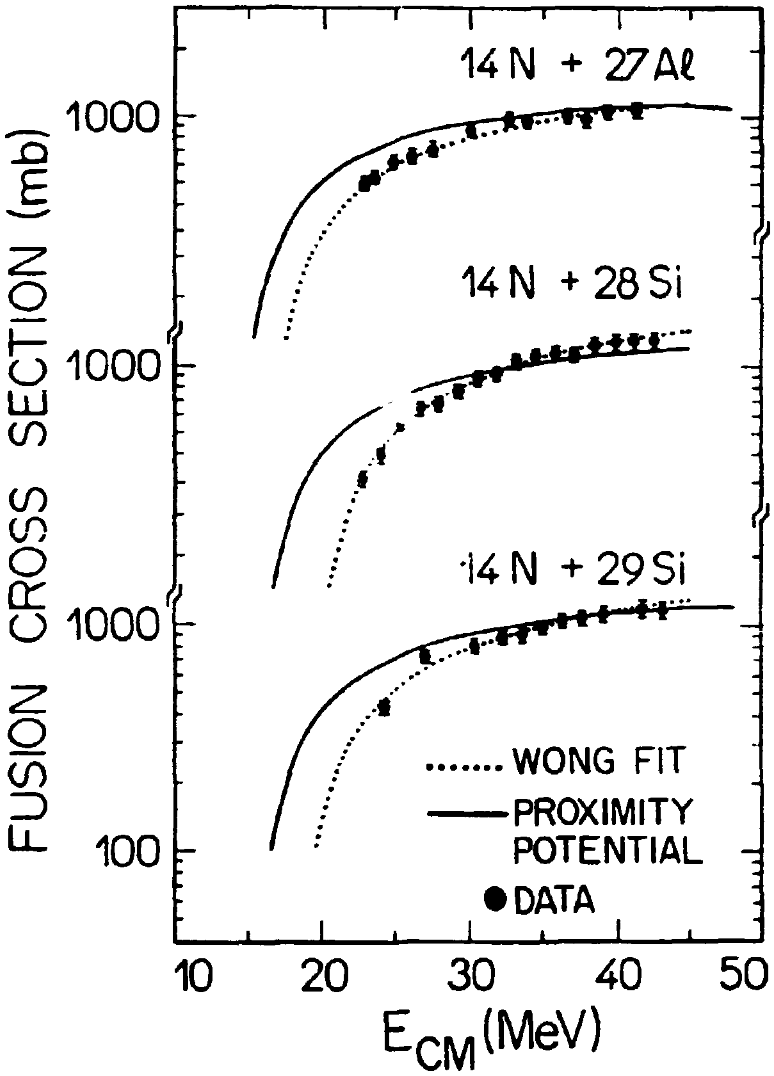

14 N + 27 Al
14 N + 28 Si
14 N + 29 Si
1000
1000
1000
100
FUSION CROSS SECTION (mb)
WONG FIT
PROXIMITY POTENTIAL
DATA
10
20
30
40
50
E_{CM} (MeV)

Figure 2

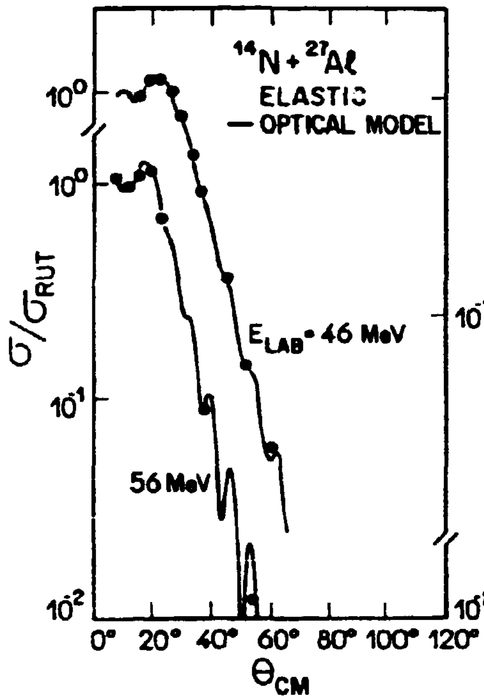

$^{14}N + ^{27}Al$
ELASTIC
— OPTICAL MODEL
E_{LAB} = 46 MeV
56 MeV
σ/σ_{RUT}
Θ_{CM}
10^0
10^0
10^{-1}
10^{-2}
10^{-1}
10^{-2}
0°
20°
40°
60°
80°
100°
120°

Figure 3a

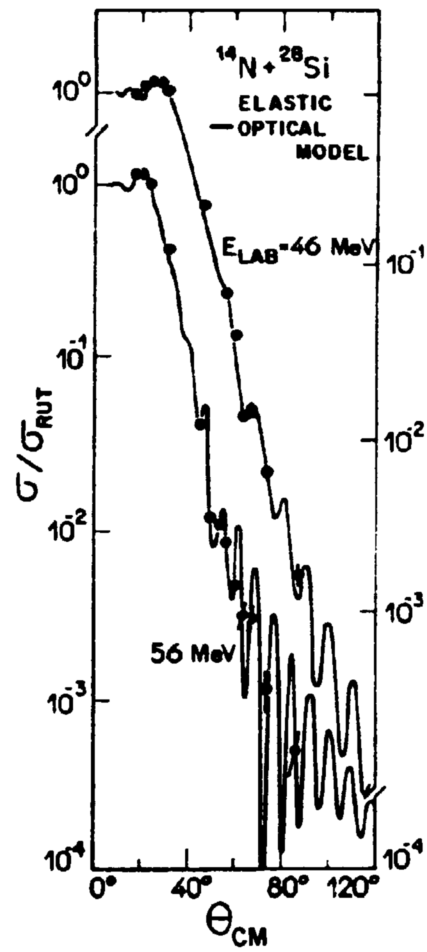

^{14}N + ^{28}Si
ELASTIC
— OPTICAL MODEL
E_{LAB}=46 MeV
56 MeV
10^0
10^0
10^{-1}
10^{-2}
10^{-3}
10^{-4}
10^{-1}
10^{-2}
10^{-3}
10^{-4}
σ/σ_{RUT}
0°
40°
80°
120°
Θ_{CM}

Figure 3b

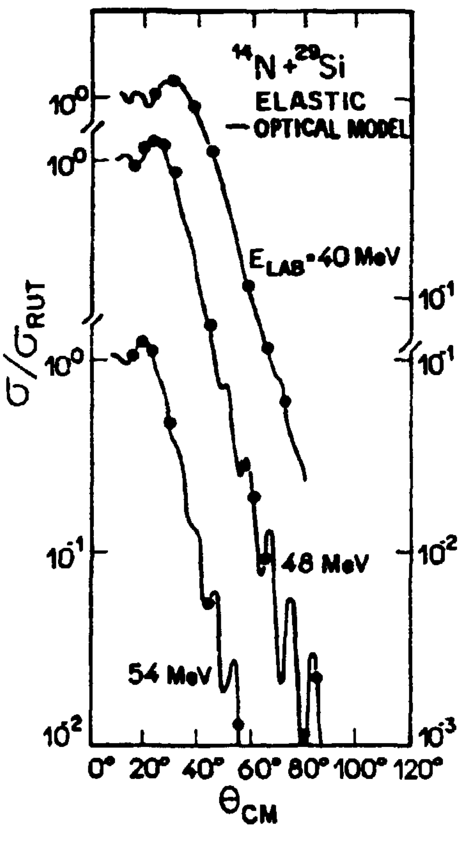

$^{14}N + ^{29}Si$
ELASTIC
— OPTICAL MODEL
E_{LAB} = 40 MeV
48 MeV
54 MeV
σ/σ_{RUT}
Θ_{CM}

Figure 3c

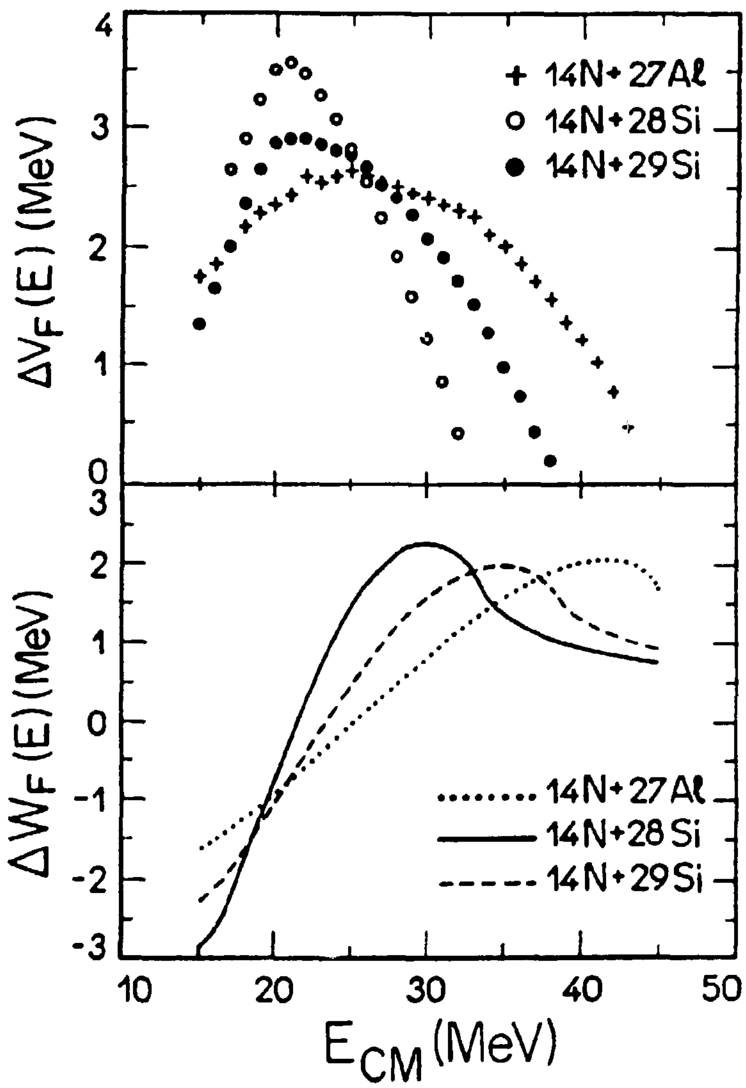

4
3
2
1
0
ΔV_F (E) (MeV)
14N+27Al
14N+28Si
14N+29Si
3
2
1
0
-1
-2
-3
ΔW_F (E) (MeV)
14N+27Al
14N+28Si
14N+29Si
10
20
30
40
50
E_CM (MeV)

Figure 4

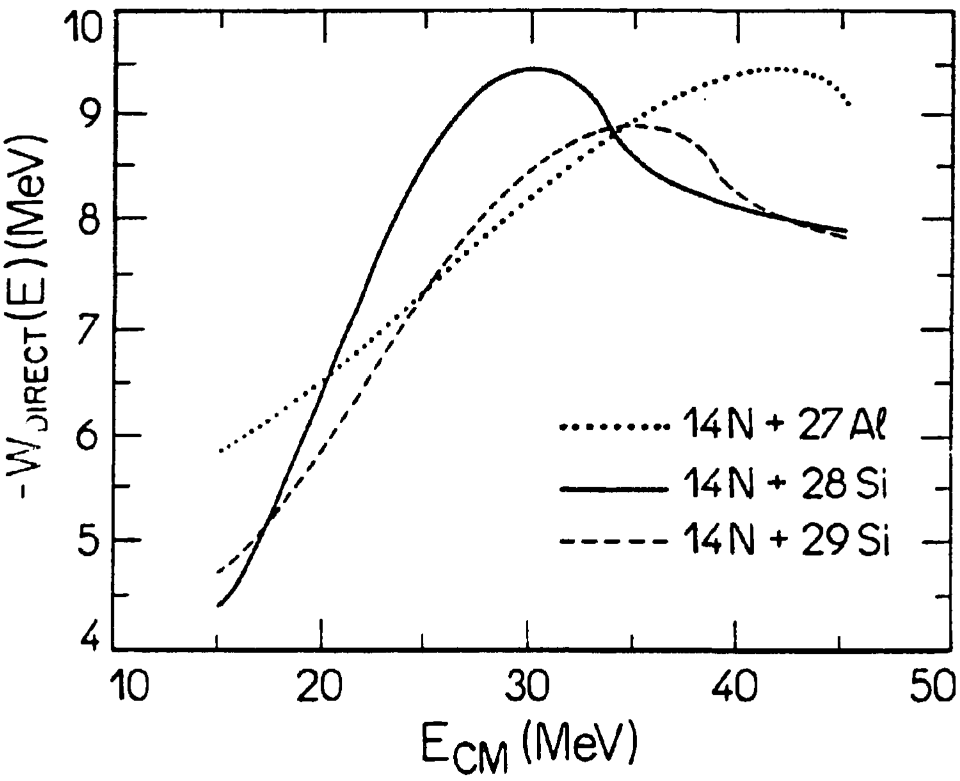

10
9
8
7
6
5
4
$-W_{DIRECT}(E)$ (MeV)
14N + 27 Al
14N + 28 Si
14N + 29 Si
10
20
30
40
50
E_{CM} (MeV)

Figure 5

	V_R(MeV)	r_R(F)	a_R(F)	V_I(MeV)	r_I(F)	a_I(F)	r_C(F)
$^{14}N+^{27}Al$	21.0	1.35	0.49	7.50	1.35	0.38	1.36
$^{14}N+^{28}Si$	21.0	1.35	0.49	7.25	1.35	0.38	1.36
$^{14}N+^{29}Si$	21.0	1.35	0.49	7.00	1.35	0.38	1.36

TABLE I - Energy independent paramete used in optical model predictions showed in figure 1.

	R_B(F)	V_B(MeV)	$\hbar\omega$(MeV)	β_{Nitrog}	β_{Alvo}
$^{14}N+^{27}Al$	7.39 ± 0.08	16.8 ± 0.2	3.6 ± 1.5	0.0	0.0
$^{14}N+^{28}Si$	8.46 ± 0.08	20.0 ± 0.1	3.4 ± 1.2	0.0	0.42 ± 0.13
$^{14}N+^{29}Si$	7.91 ± 0.09	19.0 ± 0.2	4.3 ± 1.6	0.0	0.3 ± 0.2

TABLE II - Parameters used in Wong calculation showed in figure 2. The errors reflect fit sensibility with the parameters.